Compact Tri-Band SIW Bandpass Filters With High Selectivity and Controllable Center Frequencies Using Perturbation Structure

Daotong Li, *Senior Member, IEEE*, Xiaoquan Chen, Wei Luo, Zhirui Zheng, *Student Member, IEEE*, and Qiang Chen, *Senior Member, IEEE*

***Abstract*—In this brief, two compact tri-band substrate integrated waveguide (SIW) bandpass filters (BPFs) with high selectivity and controllable center frequencies are presented based on the proposed tri-mode SIW resonant cavity perturbed by metallized vias. The resonant characteristics of the tri-mode SIW cavity are first analyzed, and the impacts of some key parameters on the resonant frequency are comparatively analyzed to further elucidate the flexible controlling of the vias perturbated SIW cavity structure. For demonstrating the superiority of the proposed tri-mode SIW cavity, a prototype of tri-band SIW BPF, centered at 11.18, 12.61 and 13.33GHz, is designed using one-layer substrate. In order to further reduce the occupied size, a tri-band SIW BPF with controllable center frequencies of 11.93, 13.21 and 14.12GHz, is constructed based on electric and magnetic coupling structure using two layers substrates. Both of the proposed tri-band BPFs exhibit six transmission zeros (TZs), resulting in good out-of-band rejections. The measured results agree well with the simulated ones.**

***Index Terms*—Substrate integrated waveguide (SIW), bandpass filter (BPF), perturbation structure, transmission zeros.**

I. Introduction

As an essential component of the RF front-end, bandpass filters (BPFs) play key roles of the entire wireless system. The traditional single passband BPFs cannot meet the requirements of miniaturization, integration, and multi-standard communication systems, and the multi-band filter is a good solution, attracting much of attention of scholars [1], [2].

Manuscript received 14 March 2023; accepted 26 May 2023. Date of publication 30 May 2023; date of current version 27 October 2023. This work was supported in part by the National Natural Science Foundation of China under Grant 61801059; in part by the FY2021 JSPS Postdoctoral Fellowship for Research, Japan, under Grant P21053; in part by the Grant-in-Aid for JSPS Research Fellow under Grant 21F21053; and in part by the Basic Research and Frontier Exploration Special of Chongqing Natural Science Foundation under Grant cstc2019jcyj-msxmX0350. This brief was recommended by Associate Editor X. Zhu. *(Corresponding author: Daotong Li.)*

Daotong Li is with the School of Microelectronics and Communication Engineering, Chongqing University, Chongqing 400044, China, and also with the Department of Communications Engineering, Tohoku University, Sendai 980-8579, Japan (e-mail: dli@cqu.edu.cn).

Xiaoquan Chen, Wei Luo, and Zhirui Zheng are with the School of Microelectronics and Communication Engineering, Chongqing University, Chongqing 400044, China.

Qiang Chen is with the Department of Communications Engineering, Tohoku University, Sendai 980-8579, Japan (e-mail: qiang.chen.a5@tohoku.ac.jp).

Color versions of one or more figures in this article are available at https://doi.org/10.1109/TCSII.2023.3281496.

Digital Object Identifier 10.1109/TCSII.2023.3281496

SIW has the advantages of high Q value, low insertion loss and easy integration, which is widely used in the miniaturization of microwave and millimeter wave active and passive devices designs [3], [4], [5].

For the SIW multi-band BPF, its design methods can be divided into the following three categories. Firstly, combining some single-band SIW BPFs into multi-band one is the straightforward approach. In [6], the dual-band BPF is realized by combining two BPFs through a dedicated impedance-matching network, however, a large circuit size is achieved. In [7], [8], multi-band BPFs are constructed by etching split-ring resonators (CSRRs) on the SIW cavity, but this method is more suitable for lower microwave frequency band. Secondly, dividing a broad passband into two or more sub-passbands through inserting transmission zeros (TZs) can also be used to design multi-band BPFs [9], [10], [11]. Although perfect symmetrical frequency responses can be obtained, the sub-passbands are usually closely adjacent and cannot be independently assigned or controlled. Thirdly, multiple bands BPF can be obtained using multi-mode resonant cavities. In [12], the SIW dual-band BPF is implemented using the TE_{101} and TE_{201} modes in a SIW cavity. Furthermore, fan-shaped SIW cavity [13], circular cavity [14], and half-mode SIW cavity [15], [16] are chosen to realize dual/tri-band BPFs. In [17], a tri-mode SIW cavity is proposed based on a perturbed structure, but lack of tunability of the resonant cavity.

In this brief, a single-layer and a double-layer SIW tri-band BPFs with different coupling topologies are implemented based on a novel tri-mode SIW resonant cavity. By loading metallized vias on the rectangle SIW cavity, the proposed tri-mode SIW cavity with three independent controllable resonant modes of TE_{101}, TE_{102} and TE_{201} can be achieved, which are validated from the electric field distribution as well as numerical analysis of the cavity. For demonstrating the superiority of the proposed tri-mode SIW cavity, a prototype of tri-band SIW BPF designed on one-layer substrate has six TZs which improve the passbands' selectivity and stopband suppressions greatly. Furthermore, for further realizing the circuit miniaturization, another tri-band SIW BPF is constructed based on electrical and magnetic coupling structure using two layers substrates. The two BPFs are designed, fabricated, and measured. The measured and simulated results agree well with each other.

This brief is organized as follows: Section II investigates the characteristics of the proposed tri-mode SIW resonator.

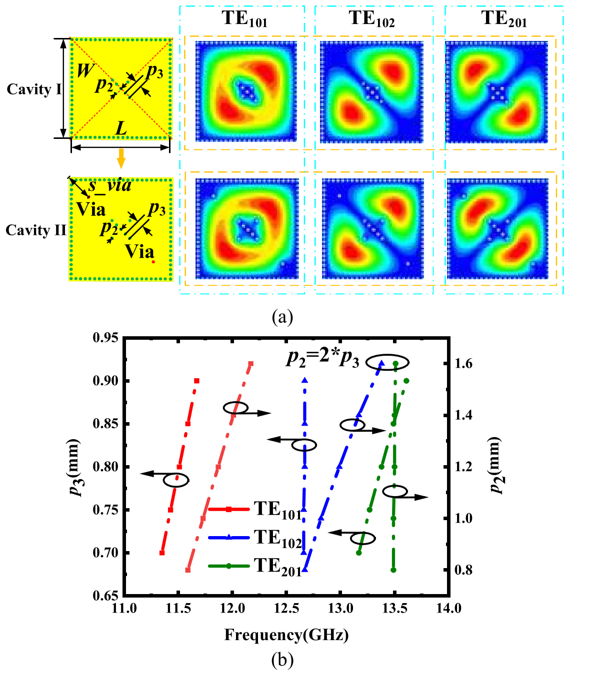

Fig. 1. (a) Geometric configuration of cavity I and cavity II, and the E-field comparison. (b) The impacts of p_2 and p_3 on frequency.

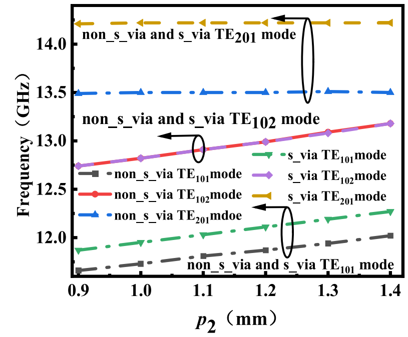

Fig. 2. Effects of p_2 on resonant frequency with or without metallized vias.

Section III demonstrates a compact tri-band SIW BPF based on the proposed tri-mode SIW cavity. In order to further realize the filter miniaturization, another tri-band SIW BPF configurations using two-layer substrates are analyzed and designed in Section IV. The conclusions are drawn in Section V.

II. Design and Analysis of Proposed SIW Resonator

In this brief, the first three resonant modes of a rectangle SIW cavity are TE_{101}, TE_{102} and TE_{201} modes, shown in Fig. 1(a), respectively. However, the three resonant modes cannot be effectively controlled, which is not easy to use in filter designs, especially in the multi-band BPF.

In order to realize the independent controllable resonant modes, a modified tri-mode SIW cavity is proposed by loading the metallized vias in the center of the structure, which is shown in Fig. 1(a). The vias are arranged along the two diagonals of the cavity with the lengths of p_2 and p_3. Firstly, the resonant frequencies of the tri-mode resonant cavity presented in Fig. 1(a) named Cavity I, can be changed by the cross-shaped metallized vias in the center of the structure. By changing the values of p_2 and p_3, the E-field distributions of the corresponding modes can be impacted. From the numerical analysis displayed in Fig. 1(b), when p_2 is fixed, the TE_{101} and TE_{201} modes can be altered by changing the value of p_3, and the TE_{102} mode remains invariable. Similarly, when p_3 is fixed, the TE_{101} and TE_{102} modes can be altered by changing the value of p_2, and the TE_{201} mode remains unchanged. When p_3 is fixed and p_2=2*p_3, the resonant frequencies of the TE_{102} and TE_{201} modes are almost the same, which would affect the realization of the tri-band response.

For further improving the adjustability of the resonant frequencies, a pair of perturbed metallized vias are added at both corners diagonally using *s_via* to mark the location, whose geometric configuration is shown in Fig. 1(a) labeled as Cavity II. From E-field distributions, it can be seen that the perturbed metallized vias are loaded at the place where the E-field distribution of TE_{102} is weakest. So, the vias mainly affect TE_{101} and TE_{201} modes, but no effect on the TE_{102} mode. As shown in Fig. 2, when the value of *s_via* and p_3 are fixed and the value of p_2 is increased, the resonant frequencies of TE_{101} and TE_{201} modes are increased, whereas the resonant frequency of TE_{102} mode remains unchanged. Compared with the case without and with the vias, the TE_{102} mode is unaffected, and the result is consistent with the E-field distribution analysis of Cavity II, while the resonant frequencies of TE_{101} and TE_{201} are shifted about 200MHz and 800MHz, respectively, because of the perturbation vias. Therefore, by diagonally loading a pair of perturbed metallized vias on the cavity, the adjustability of the TE_{201} model is improved. In summary, by combining the above key parameters including p_2, p_3, and *s_via*, the resonant frequencies of TE_{101} TE_{102} and TE_{201} modes in the single SIW cavity can be controlled independently.

III. Single-Layer SIW Tri-Band BPF Design

A. Filter Configuration

The configuration of the proposed SIW tri-band BPF by cascading two tri-mode cavities with a single-layer substrate is shown in Fig. 3(a). Fig. 3(b) illustrates the corresponding coupling topology diagram, where A, B and C represent TE_{101}, TE_{102} and TE_{201} modes, separately. Two transmission zeros beside the two sides of each passband are introduced by source-load coupling (SLC) structure, resulting in high selectivity and high rejection. The comparison of the proposed BPF with and without SLC structure is illustrated in Fig. 4, it can be found that three additional transmission zeros can be introduced.

B. Parameters Analysis

The couplings of the three modes in each cavity can be adjusted by two coupling windows shown in Fig. 3(a). w_2 and w_3 donate the width of the upper and lower coupling windows. From the E-field distributions in Fig. 1(a), the upper window is designed for mutual couplings of TE_{101} and TE_{102} modes, while the lower window is used for controlling the couplings of TE_{101} and TE_{201} modes. The coupling coefficient K_{ij} *(j>i)*

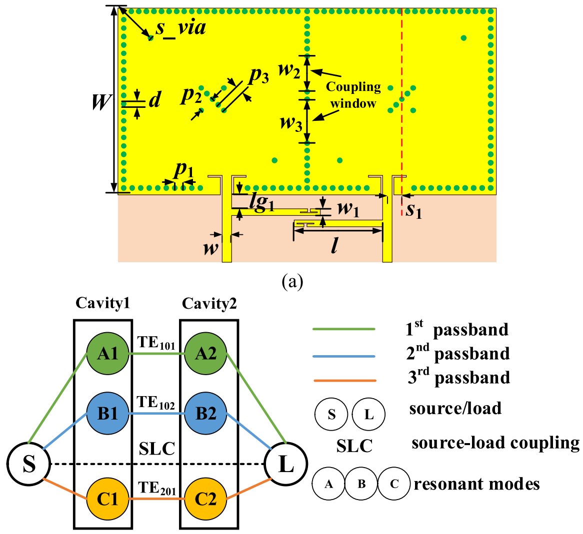

Fig. 3. Proposed single-layer SIW tri-band BPF. (a) Geometric configuration, (W=20, s_via=3.45, d=0.6, p_1=0.9, p_2=1.2, p_3=0.6, lg_1=1.5, w_1=0.7, w_2=3.8, w_3=4.7, l=9.36, s_1=1.52. Unit.mm). (b) Coupling topology.

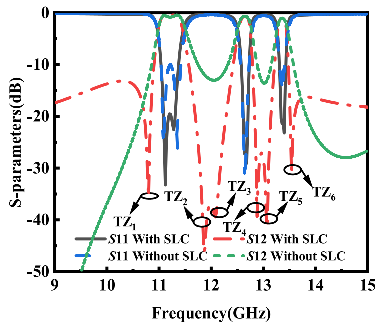

Fig. 4. Simulated S-parameters with and without SLC structure.

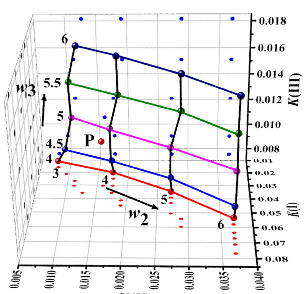

Fig. 5. Extracted coupling coefficients of the cascaded SIW tri-mode cavities.

between the two modes can be evaluated by [18]

$$K_{ij} = \frac{f_j^2 - f_i^2}{f_j^2 + f_i^2} \tag{1}$$

where f_i and f_j (j>i) denote the corresponding resonant frequencies of proposed tri-band SIW cavity.

Fig. 5 shows the impacts of w_2 and w_3 on the coupling coefficients. K(I), K(II), and K(III) denote the coupling coefficients of TE_{101}, TE_{102} and TE_{201} modes between the two cascaded SIW cavities, respectively. It can be observed that K(I) and K(II) increase as w_2 increases, while K(III)

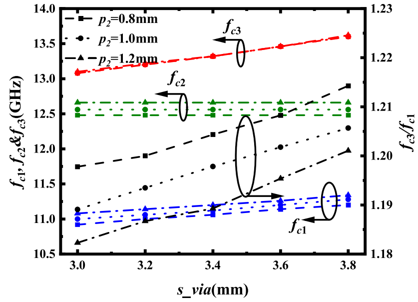

Fig. 6. Impact of parameter p_2 on center frequency of each passband.

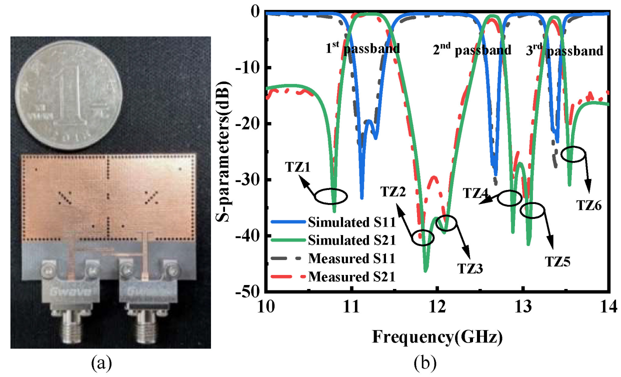

Fig. 7. (a) Photograph of the fabricated single-layer SIW BPF. (b) Simulated and measured S-parameters of the proposed BPF.

remains almost unchanged. When w_3 increases, K(I) and K(III) increase with little influence on K(II). Thus, the coupling coefficients of TE_{101} and TE_{102} modes are attributed to the upper coupling window, and the coupling coefficients of TE_{101} and TE_{201} modes are mainly affected by the lower coupling window.

To clearly indicate the impacts of perturbation vias, the relationships between the parameters s_via and p_2 and the resonant frequencies are investigated, as shown in Fig. 6. By raising the value of s_via, the center frequencies of the first passband f_{c1} and the third passband f_{c3} are increased, while the center frequency of the second passband f_{c2} is not affected. Moreover, when the value of p_2 becomes larger, the first and second passbands are increased, while the third passband is not influenced. Therefore, based on the aforementioned analysis, the proposed BPF has controllable frequency ratios, operating center frequencies and bandwidths.

C. Simulated and Measured Results

In order to validate the design approach, a prototype of single-layer tri-band BPF is designed, fabricated and measured. The photograph of the fabricated tri-band BPF is shown in Fig. 7(a). The substrate used in this design is Rogers RT/Duriod 5880 substrate with the relative dielectric constant ε_r= 2.2, thickness h = 0.508 mm, and loss tangent tanδ = 0.0009. Fig. 7(b) indicates the measured/simulated results of the S-parameters of the tri-band BPF in the frequency range from 10 to 14 GHz. The measured/simulated results show that the center frequencies of the three passbands of the proposed tri-band BPF are 11.18/11.20 GHz, 12.6/12.64 GHz and 13.33/13.36 GHz, respectively. The

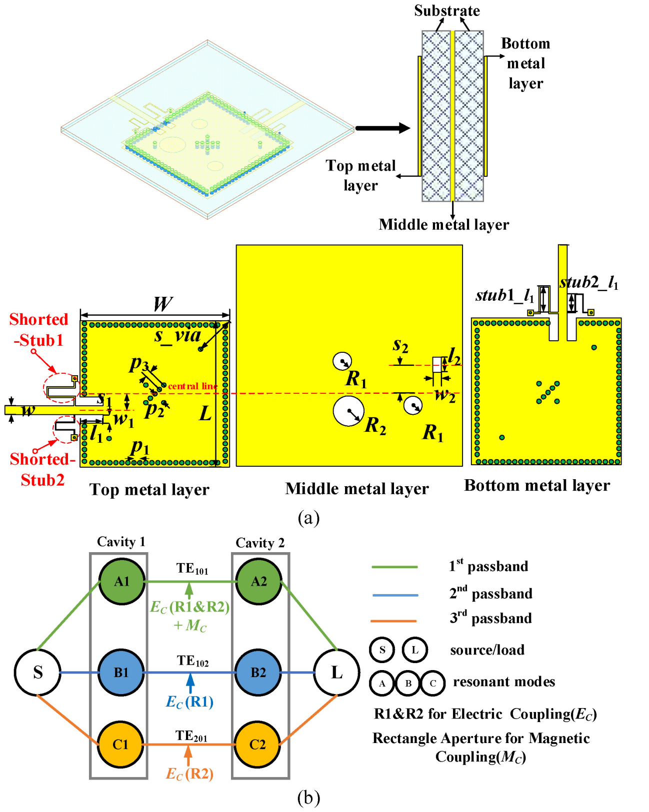

Fig. 8. Configuration of the double-layer SIW tri-band BPF. (a) 3D View. (W=20, L=20, s_via=3.9, d=0.6, p_1=0.9, p_2=1.2, p_3=0.6, l_1=3.1, w=1.2, w_1=1.2, w_2=1.2, l_2 = 2.2, R_1=1.3, R_2=2.17, s_1=2.2, s_2=2.7, $stub2\_l_1$=2.4, $stub1\_l_1$=3.8. Unit.mm). (b) Coupling topology.

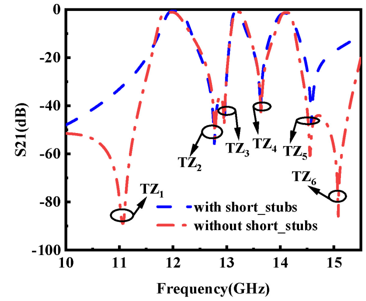

Fig. 9. Transmission coefficients of the proposed tri-band BPF with and without shorted stubs.

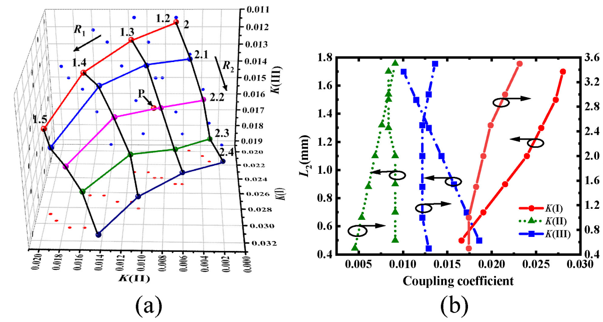

Fig. 10. Extracted coupling coefficients, (a) K(I), K(II) and K(III) against varied R_1 and R_2. (b) K(I), K(II) and K(III) versus changed L_2 and s_2.

return losses of the passbands are better than 19.49/19.5 dB, 31.5/25.9 dB and 27.6/21.3 dB, respectively. The minimum in-band insertion losses are 0.55/0.43 dB, 1.56/0.73 dB and 1.78/0.97 dB, separately. Six transmission zeros are located at 10.81/10.8 GHz, 11.82/11.86 GHz, 12.1/12.08 GHz, 12.9/12.88 GHz, 13.04/13.06 GHz and 13.52/13.54 GHz, improving the frequency skirt selectivity and out-of-band rejection greatly. The measured fractional bandwidths (FBWs) are 3.93%, 1.91% and 1.43%, respectively. The measured results agree well with the simulation results.

IV. Double-Layer SIW Tri-Band BPF Design

To further miniaturize the filter structure and verify the performance of the resonant cavity, the configuration of Fig. 3(a) is folded and coupled through different apertures to realize a double-layer SIW tri-band BPF.

A. Filter Configuration

Fig. 8(a) shows the 3D View of the double-layer tri-band SIW BPF. The cavities are vertically coupled with mixed electric and magnetic couplings through the apertures, and the corresponding coupling topology is shown in Fig. 8(b). According to the E-field distribution in Fig. 1(a), the first passband consists of the TE_{101} modes mainly coupled by electric couplings through the R_1 and R_2 circular and rectangle apertures. Similarly, the third passband is composed of the TE_{201} modes coupled through the R_2 circular aperture. The TE_{102} modes coupled through the R_1 circular apertures are utilized to generate the second passband. Besides, a controllable transmission zero (TZ_2) is introduced by the canceling effect of mixed electric and magnetic coupling through the circular and rectangular apertures [19]. In addition, to further improve the out-of-band rejection performance of the proposed tri-band BPF, two pairs of quarter-wavelength shorted-stubs are loaded at the input and output ports to generate two extra transmission zeros (TZ_1 and TZ_6), as shown in Fig. 9.

B. Parameters Analysis

Fig. 10(a) presents the variations of K(I), K(II) and K(III) versus the key parameters R_1 and R_2. As the value of R_1 increases, K(I) and K(II) rise as a whole, while K(III) is almost unchanged, which is because the first and second passbands are mainly coupled by R_1. When the value of R_2 increases, K(I) and K(III) become larger as a whole, while K(II) decreases. This is because the E-field distribution of the TE_{102} mode would be impacted by the size of R_2 circular aperture, shown in Fig. 1(a). In Fig. 10(b), when s_2 is fixed, the larger of L_2, the greater of K(I), and the smaller of K(III), while K(II) maintains almost unchanged. Moreover, when L_2 is fixed and s_2 is increased, both the K(I) and K(II) are increased, while K(III) almost keeps the same. Thus, the couplings of the upper and lower cavities can be controlled by combining the analysis of the coupling apertures parameters R_1, R_2, L_2 and s_2.

C. Simulated and Measured Results

For demonstration, a prototype of the proposed double-layer tri-band BPF is designed, simulated, fabricated and measured. Fig. 11(a) shows the photograph of the fabricated double-layer tri-band BPF. Fig. 11(b) indicates the measured/simulated

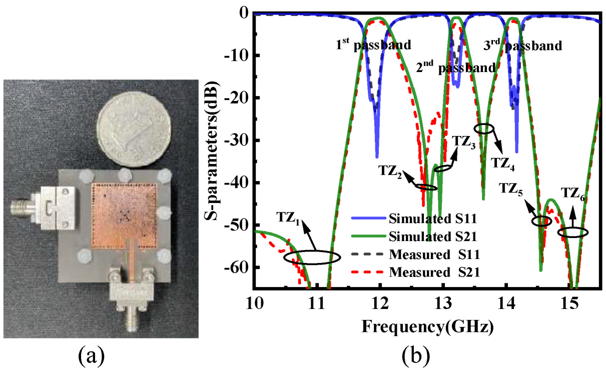

Fig. 11. (a) Photograph of the fabricated double-layer SIW BPF. (b) Simulated and measured S-parameters of the proposed tri-band BPF.

TABLE I
COMPARISONS WITH OTHER REPORTED SIW BPFS

Ref	Structure	f_0*(GHz)	TZ	IL*(dB)	Size(λ_g^2)
[3]	Double layer	1.83/2.1/2.47	6	2.31/2.25/3.01	0.22×0.22
[10]	Single layer	11.58/12.47/14.9	5	0.84/0.9/1.03	2.14×2.14
[11]	Triple layer	18.7/19.1/19.8	4	0.98/0.67/1.4	1.15×1.15
[14]	Single layer	13/14/15	3	1.71/1.80/2.29	3.38×1.19
This work	**Single layer**	**11.18/12.6/13.33**	**6**	**0.55/1.56/1.78**	**2.20×1.38**
	Double layer	**11.92/13.23/14.1**	**6**	**1.81/2.35/1.93**	**1.65×1.65**

f_0* denotes the center frequencies of the tri-band BPF; IL* represents insertion loss.

results of the S-parameters of the double-layer tri-band SIW BPF in the frequency range from 10 to 15.5 GHz. The center frequencies of the three passbands of the proposed tri-band SIW BPF are 11.92/11.93 GHz, 13.23/13.21 GHz and 14.1/14.12 GHz, respectively. The minimum in-band insertion losses are 1.81/1.31 dB, 2.35/1.09 dB and 1.93/1.30 dB, respectively. Six transmission zeros are located at 11.04/11.06 GHz, 12.68/12.78 GHz, 13.03/12.95 GHz, 13.64/13.63 GHz, 14.57/14.55 GHz and 15.06/15.08 GHz. The measured FBWs are 2.85%, 1.29% and 1.42%, respectively. The measured results are consistent with the simulation results.

The comparisons between our designs and some recent reported SIW BPFs are listed in Table I. It can be concluded from the comparison table that the proposed tri-band BPF has lower in-band insertion loss and occupies a smaller size. Moreover, six TZs can be obtained enabling the proposed tri-band BPF to achieve better out-of-band rejection performance. These comparisons reveal that the proposed ones are good candidates for the wireless communication application.

V. CONCLUSION

This brief presents two compact SIW tri-band bandpass filters based on the proposed novel SIW tri-mode cavity. By adjusting the perturbation structure, the resonant characteristics of the multi-mode cavity can be easily controlled to realize flexible adjustability. Based on the proposed tri-mode SIW cavities, a single-layer SIW tri-band BPF with SLC structure is achieved. Moreover, to further improve the integration and miniaturization, the SIW tri-band BPF with shorted-stubs using double-layer substrate is constructed. Both of the BPFs have six TZs, which results in high selectivity and out-of-band rejections. The proposed tri-band BPFs are fabricated and measured, and the measured results agree well with simulated values. Because of those merits, the designed two tri-band BPFs are good candidates for multi-band transceiver systems.

REFERENCES

[1] A. Iqbal, J. J. Tiang, S. K. Wong, M. Alibakhshikenari, F. Falcone, and E. Limiti, "Miniaturization trends in substrate integrated waveguide (SIW) filters: A review," *IEEE Access*, vol. 8, pp. 223287–223305, 2020.
[2] H.-W. Xie, K. Zhou, C.-X. Zhou, and W. Wu, "Compact SIW diplexers and dual-band bandpass filter with wide-stopband performances," *IEEE Trans. Circuits Syst. II, Exp. Briefs*, vol. 67, no. 12, pp. 2933–2937, Dec. 2020.
[3] H. Zhang, W. Kang, and W. Wu, "Miniaturized dual-band SIW filters using E-shaped slotlines with controllable center frequencies," *IEEE Microw. Wireless Compon. Lett.*, vol. 28, no. 4, pp. 311–313, Apr. 2018.
[4] M.-H. Ho and K.-H. Tang, "Miniaturized SIW cavity tri-band filter design," *IEEE Microw. Wireless Compon. Lett.*, vol. 30, no. 6, pp. 589–592, Jun. 2020.
[5] A. R. Azad and A. Mohan, "Single- and dual-band bandpass filters using a single perturbed SIW circular cavity," *IEEE Microw. Wireless Compon. Lett.*, vol. 29, no. 3, pp. 201–203, Mar. 2019.
[6] S. Y. Zheng, Z. L. Su, Y. M. Pan, Z. Qamar, and D. Ho, "New dual-/tri-band bandpass filters and diplexer with large frequency ratio," *IEEE Trans. Microw. Theory Techn.*, vol. 66, no. 6, pp. 2978–2992, Jun. 2018.
[7] H. Zhang, W. Kang, and W. Wu, "Miniaturized dual-band differential filter based on CSRR-loaded dual-mode SIW cavity," *IEEE Microw. Wireless Compon. Lett.*, vol. 28, no. 10, pp. 897–899, Oct. 2018.
[8] W. Fu, Z. Li, P. Liu, J. Cheng, and X. Qiu, "Modeling and analysis of novel CSRRs-loaded dual-band bandpass SIW filters," *IEEE Trans. Circuits Syst. II, Exp. Briefs*, vol. 68, no. 7, pp. 2352–2356, Jul. 2021.
[9] K. Zhou, C.-X. Zhou, H.-W. Xie, and W. Wu, "Synthesis design of SIW multiband bandpass filters based on dual-mode resonances and split-type dual- and triple-band responses," *IEEE Trans. Microw. Theory Techn.*, vol. 67, no. 1, pp. 151–161, Jan. 2019.
[10] P. Li, H. Chu, and R.-S. Chen, "Design of compact bandpass filters using quarter-mode and eighth-mode SIW cavities," *IEEE Trans. Compon. Packag. Manuf. Technol.*, vol. 7, no. 6, pp. 956–963, Jun. 2017.
[11] K. Zhou, C. Zhou, and W. Wu, "Substrate-integrated waveguide triple-band filter with improved frequency and bandwidth allocations," *Electron. Lett.*, vol. 54, no. 19, pp. 1132–1134, Sep. 2018.
[12] X. Zhou, G. Zhang, J. Zheng, W. Tang, and J. Yang, "SIW filter with adjustable number of passbands using assembled multimode resonant PCBs," *IEEE Trans. Circuits Syst. II, Exp. Briefs*, vol. 69, no. 8, pp. 3386–3389, Aug. 2022.
[13] Y.-K. Han, H.-W. Deng, J.-M. Zhu, S.-B. Xing, and W. Han, "Compact Dual-band dual-mode SIW balanced BPF with intrinsic common-mode suppression," *IEEE Microw. Wireless Compon. Lett.*, vol. 31, no. 2, pp. 101–104, Feb. 2021.
[14] S. Zhang, J.-Y. Rao, J.-S. Hong, and F.-L. Liu, "A novel dual-band controllable bandpass filter based on fan-shaped substrate integrated waveguide," *IEEE Microw. Wireless Compon. Lett.*, vol. 28, no. 4, pp. 308–310, Apr. 2018.
[15] Z. Zheng, X. Tan, D. Li, and Q. Chen, "A single-layer dual-band shielded HMSIW bandpass filter using single SIW cavity," *AEU Int. J. Electron. Commun.*, vol. 154, Sep. 2022, Art. no. 154337.
[16] B.-G. Liu, Y.-P. Lyu, L. Zhu, and C.-H. Cheng, "Compact single- and dual-band filters on hexa-modes half-mode substrate integrated waveguide resonator with loaded H-shaped slot," *IEEE Microw. Wireless Compon. Lett.*, vol. 30, no. 12, pp. 1129–1132, Dec. 2020.
[17] H.-W. Xie, K. Zhou, C.-X. Zhou, and W. Wu, "Substrate-integrated waveguide triple-band bandpass filters using triple-mode cavities," *IEEE Trans. Microw. Theory Techn.*, vol. 66, no. 6, pp. 2967–2977, Jun. 2018.
[18] J.-S. Hong and M.-J. Lancaster, *Microstrip Filters for RF/Microwave Applications*. New York, NY, USA: Wiley, 2001, ch. 8.
[19] Z. L. Su, B. W. Xu, S. Y. Zheng, H. W. Liu, and Y. L. Long, "High-isolation and wide-stopband SIW diplexer using mixed electric and magnetic coupling," *IEEE Trans. Circuits Syst. II, Exp. Briefs*, vol. 67, no. 1, pp. 32–36, Jan. 2020.